HTMS Report

Greg Sakradse, Sarah Smith and Raúl Bayoán Cal
Dept. Mechanical & Materials Engineering
Portland State University

1 Outdoor air mitigation and site fluid mechanics

Urban forests are often proposed as a means of ameliorating air pollution in cities. While studies that investigate the city-scale indicate generally positive effects of urban vegetation on air quality Yang et al. (2008), local effects of barriers (often vegetation, but also abiotic structures like sound walls) are mixed in terms of mitigation benefit in the research literature. For example, recent studies have come to conclusions that show street level vegetation as increasing (Vos et al. (2013); Wania et al. (2012)) or decreasing (Abhijith and Gokhale (2015); Pugh et al. (2012)) local concentrations of air pollutants. The Environmental Protection Agency promulgates a summary of recommendations for the use of roadside vegetation barriers to improve near-road air quality, noting that "studies have shown that noise and vegetative barriers can reduce downwind pollutant concentrations near roads" and offer recommendations for constructing roadside barriers to optimize the downwind reduction in air pollution emitted to vehicular traffic (ORD US EPA 2016).

Studies of the impact of urban vegetation are carried out from fundamental as well as applied perspectives. Urban forests were incorporated in Beijing, Los Angeles, Sacramento and Salt Lake City, and showing a direct impact in decreasing local pollution as shown by Yang et al. (2005), Akbari (2002). On the side of noise, strategies have been proposed in a careful implementation by considering parametric studies of tree placement, foliage, density of trees, and orientation depending on the source. Such strategies can be considered in the proposed work. In addition, Cal has recently been funded to work on non-homogeneous forest canopies with aim to understand weather forecasting and deforestation. Of relevance, strategies integrated in different studies (summarized by Janhäll (2015)) have yielded a percentage decrease in PMs on the order of 40%; approaches in the proposed study could improve upon these. Within this review, works pointing towards the possible strategies and improvements specifically in areas where roadsides are present. Perhaps the most relevant, Hagler et al. (2012), provide comparisons of various barrier composed of trees or brick. Benefits were achieved yet were site and wind condition dependent.

In considering an even more recent review, Abhijith et al. (2017) evaluates a more comprehensive set of conditions both in the field and wind tunnel settings. As concisely stated in the abstract: "For open road conditions, wide, low porosity and tall vegetation leads to downwind pollutant reductions while gaps and high porosity vegetation could lead to no improvement or even deteriorated air quality. The review considers that generic recommendations can be provided for vegetation barriers in open road conditions." Remediation via vegetation is systematically discussed in Baldauf (2017) where comments on height, porosity, thickness, length and coverage are within the parameter space when considering its design and implementation. Solid barriers are reviewed in a like article, Gallagher et al. (2015), as that by Abhijith et al. (2017). Similar approaches are evaluated and conclude: "Measurement studies and modelling investigations have found relatively consistent reductions in pollutant concentrations downwind of the barriers. However, similar to the roadside vegetation studies, an increase in upwind concentrations has been identified due to the recirculation of pollutants in the zone in front of the structure. ... reattachment of a plume downwind of a barrier could lead to higher concentrations further downwind of the barrier compared to no barrier under some settings.

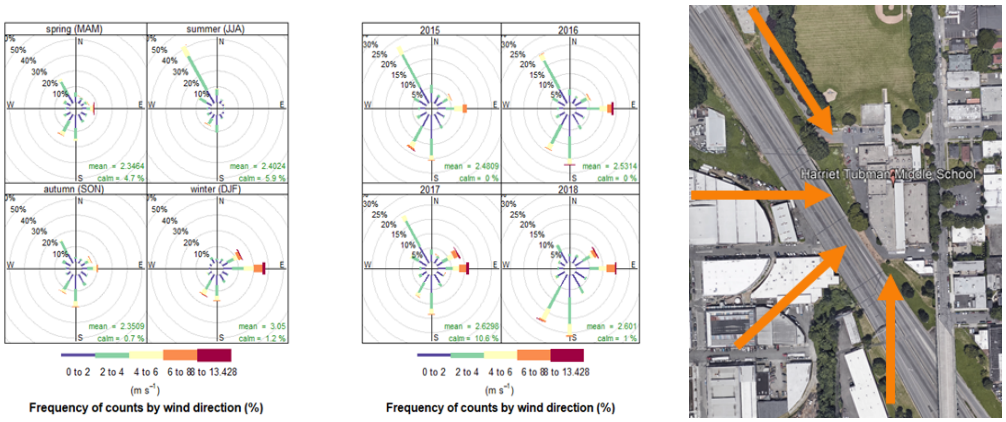

(a) (b) (c)

Figure 1: (a) and (b), Predominant wind directions as reported at Southeast Lafayette station; (c)

The height and layout of the noise barrier... presented the greatest influence on the dispersion of pollutants along the highway." Indeed, this should be deemed as relevant here in this study. It is noted that numerous studies are consulted when crafting these reviews for which further detail and information may be extracted.

1.1 Model design and manufacturing

The key parameters informing the design of the model used in this study are the mean wind direction and an appropriate length scale. Information regarding the average wind speed and directions were made available from the Southeast Lafayette weather station over a four year period between 2014-2018 and averaged for each season over the time period. Weather station data show directional predominance coming from the northwest, southwest, south, and easterly directions, with average velocities in the range of 2-4 m/s as represented in Figures 1(a) and 1(b). In order to fully capture the dynamic wind effects with respect to freeway particulates, the eastern wind direction has been replaced by an additional western plane direction. All four considered directions are shown with reference to the school in Figure 1(c).

The topography and architecture surrounding the site is represented at a scale of 1:120 for the purposes of this study. A scale of 1:120 was chosen to provide the highest possible resolution in describing the wind flow surrounding the site with the equipment at the Portland State University (PSU) wind tunnel. Additionally, this scale considers the influence of major obstacles located upstream of the mean wind for each prominent direction.

LIDAR data was acquired from the 2014 Oregon Department of Geology and Mineral Industries (DOGAMI) LIDAR survey for the area of interest depicted in figure 2a. The LIDAR data contains three dimensions of measurement accurate to approximately 1m and is used as the basis for model construction. The LIDAR data was analyzed with GIS software, Geographical Information System (GIS) software and a 3D model was developed as shown in figure 2a. Elevation slices were defined from the 3D model such that each slice represents a 0.5m change in elevation.

In the process of model creation, the elevation slices were cut out of 4mm thick cardboard and layered to create a scaled physical model of the topography surrounding Tubman Middle School. An example of the construction process is shown for the south direction in Figure (3). Upon aligning layer assembly, the model was be coated with papier-mâché to smooth out any ridges present as a result of the layering method used. Dimensions of the school and its surrounding buildings were also identified via GIS LIDAR data and model structures were defined using 3-d modeling software. Models of the school and relevant structures have

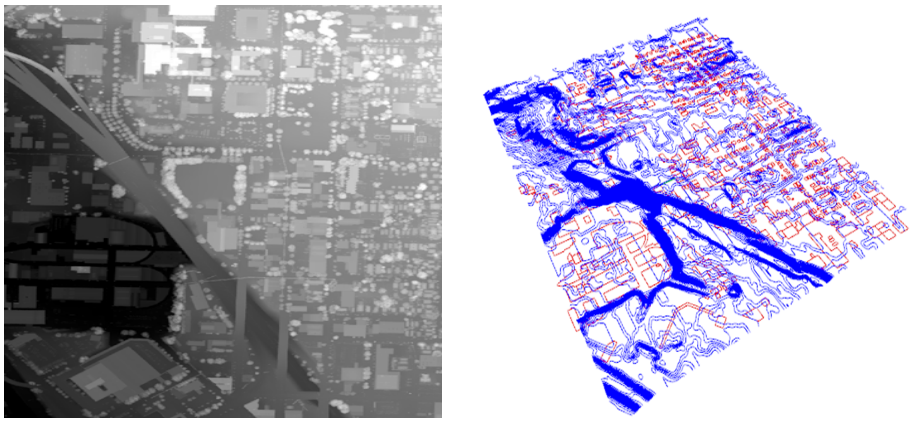

(a) (b)

Figure 2: Acquisition and modelling surrounding area: (a) LIDAR image of Tubman elimentry and surrounding area; (b) Processed topographical representation. Elevation contours each line represents a 0.5 m elevation change. Topography model is made of layers per the contours.

been separately fabricated and fixed to the topography in their precise locations determined via the LIDAR survey.

The proposed scale model of Harriet Tubman Middle School (HTMS) and relevant surroundings was situated in the 1.2 m by 0.8 m by 5.0 m wind tunnel at Portland State University. Data collection was taken via stereo particle image velocimetry (PIV). In this technique, a planar laser sheet is generated to illuminate particles and capture snapshots of these using two high-resolution cameras to produce instantaneous, three-dimensional velocity flow fields within the interrogation area.

The laser sheet plane was situated to agree with the direction of each respective wind direction and aligned perpendicular to the school site to capture flow statistics. Two separate planes are considered for each wind direction: one approaching the school to observe the effects of topography on incoming flow, and one over a portion of the school itself. An example of the two planes is shown for the south inflow direction in Figure (4), where the 'over school' plane is positioned over the HTMS basketball court. All other over school planes are positioned over the main school building in the direction of flow. Due to the topographical diversity between the four directions each plane has a slightly varied interrogation window size. To fully capture relevant dynamics and length scales all approaching planes contain the area at the ground and up to at least 4m above the building roof, and a minimum height of 10m is considered above the roof for all cases taken over the school structures.

1.2 Experimental cases

Four separate topographical configurations were considered for each of the 8 planes, resulting in a total of 32 cases for the study. The four configurations are shown in Figure (5) and were chosen to compare the current freeway and school configuration (Figure 5a) to varied combinations of proposed changes to the site: The un-altered I-5 freeway with a freeway wall implemented along the edge of school property (b), a proposed expansion of two new lanes (7.2m) added to the I-5 freeway width next to the school (c), and the proposed expansion with the additional freeway wall (d).

(a)

(b)

Figure 3: (a) Topographic 3d modelling representation of studied area, satellite image of the same image, and the area in cardboard layers. (b) The final model with roads and buildings placed, and a view in the wind tunnel

1.3 Results

The wind tunnel measurements using particle image velocimetry produce three-dimensional velocity data which is specified as u, v, and w, for velocity in the streamwise, vertical, and in plane directions, respectively. In order to gain some insight into relevant flow dynamics, the instantaneous velocity for each directional component is decomposed into a mean velocity at each point and the respective fluctuations about that mean. For all subsequent analysis, mean velocities are here denoted by an overbar ($\bar{u}\,\bar{v}$, and $\bar{w}$) and velocity fluctuations are specified with a prime (u', v' and w'). These measurements are broken out by orientation as shown in figure 1. It should be noted that the experiments performed are highly idealized and simplified as the flow observed by HTMS is much more complex, prone to variations such as changes in wind direction, atmospheric conditions, local topography to name a few.

1.3.1 Mean velocities

Figures 6 through 13 show contours of the out of plane component, $\bar{w}$, and streamlines composed of $\bar{u}$ and $\bar{v}$, for all locations as detailed previously. Each figure contains the four geometries tested (pre-expansion no

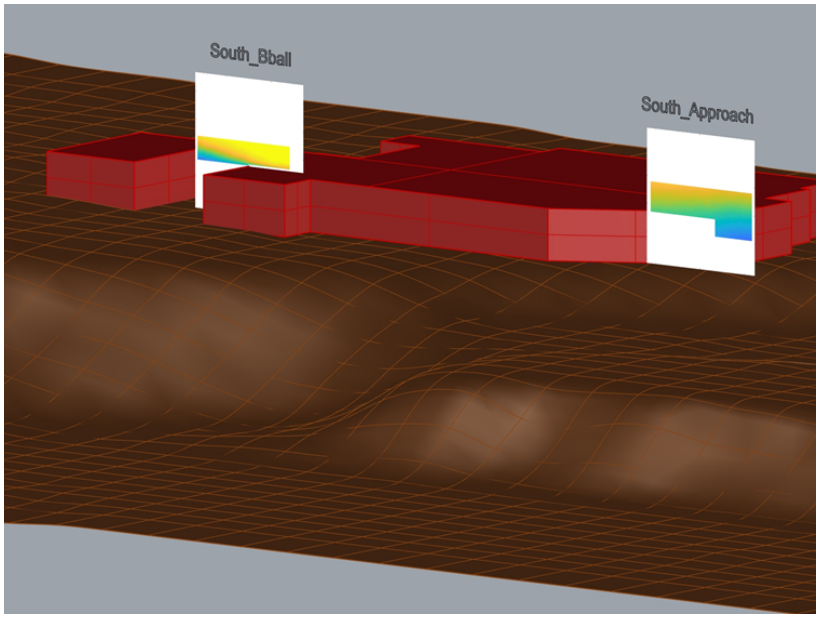

Figure 4: Example of planar data collection locations within two separate planes, here for the south wind direction. The plane titled South_Approach captures incoming flow as it approaches the structure of the school, South_Bball represents flow dynamics between the main building and approaching the school basketball court.

wall, pre-expansion wall, post-expansion no-wall and post-expansion wall). The aim is to assess fields of the mean flow in regards to the various modifications. The most relevant features are discussed.

On figure 6, local effects induced by the wall are observed as the streamlines are slightly deflected upwards near the building. This also induces a stronger out-of-plane mean velocity as indicated by the mean velocity. This is consistent with continuity as variations in a particular component should be compensated by the others. Yet note that these variations are *on average* roughly twice in magnitude. This also points towards the three dimensionality caused by the geometry. Higher vertical velocities are observed earlier due to the wall Slightly smaller magnitudes are observed towards the end of the streamlines in the interrogation areas which consider a wall. This case and flow field can be considered to be the inflow to that being advected over the basketball court as shown in figure 7. Further, strong vertical velocities are observed when a wall is present in the basketball court yet the streamwise velocity component shows slight differences.

Following figure 7, small differences for the various cases are observed in all velocity components for southern winds over the basketball court. Nevertheless, it should be noted that this considers the flow from the south predominantly which crosses over the roof of the school prior to the basketball court. Furthermore, the out-of-plane component towards HMTS is observed here, where the geometry induces negative (into the

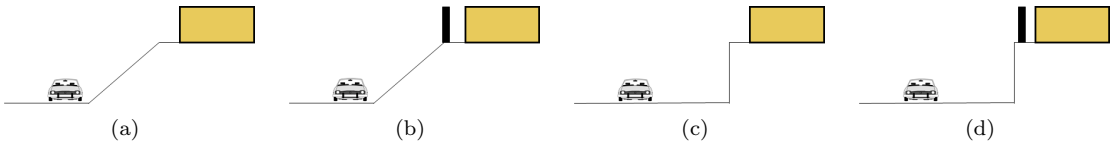

Figure 5: Freeway and obstacle configurations: (a) Pre-expansion, No Wall; (b) Pre-expansion, Wall present; (c) Post-expansion, No Wall; (d) Post-expansion, Wall

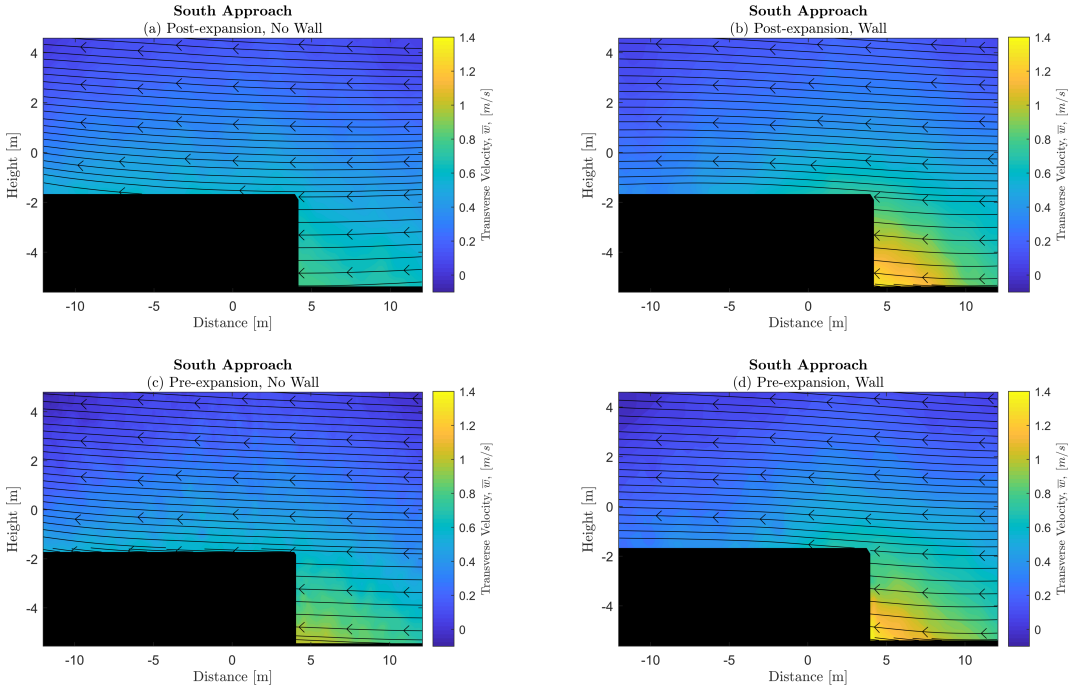

Figure 6: Streamlines of mean in plane velocity components, $\bar{u}$, and $\bar{v}$ overlaid on the mean out of plane velocity, $\bar{w}$ for the south approach view.

page) crossflow in the lower portion of the interrogation area.

The northwestern approach considers the incoming winds nearest to the park north of HTMS and is shown in figure 8. Here, changes in the expansion state alone shows little difference in the streamline behavior and a small positive (out of page) enhancement to the in plane component appears for the no wall cases. The most significant effect is seen here between the pre-expansion no wall and wall cases, where an increase of more than double in the out of plane crossflow is coupled with a slightly curved redirection of streamlines denoting an effect by the wall. Note that the post-expansion cases show a much more subtle response to the presence of the wall than pre-expansion and produce lower magnitudes of crossflow velocities in the approaching region. This behavior suggests that the pre-expansion configuration is more sensitive to the changes invoked by the presence/absence of a wall. In the other components, a decrease in the vertical velocity is observed due to the presence of the wall while differences in the streamwise velocity are more difficult to determine.

Northwestern winds over the main school building show the most prominent differences between the two expansion configurations as in figure 9. Wall presence has a negligible effect on both the streamline and in plane velocity components for the pre-expansion case. However, for the post-expansion configuration, there is an observable difference relating to the presence of the wall. Streamline velocities do not appear to change drastically between the two treatments, but the no wall case shows visibly higher in plane velocities than with a wall present. The presence of the wall may be working to regulate flow behavior over the structure for the post-expansion case. The vertical and streamwise differences in the velocity are difficult to determine.

When considering the southwest direction the expansion state seems to play a minor effect compared to wall presence, which introduces a strong into-the-plane velocity for the pre-expansion case as shown in figure 10. The streamlines are affected as the flow tends to have further curvature above the wall. Note that the terrain plays a relevant role here as streamlines are generally directed upwards. Magnitudes are relatively less when a wall is present. The maximum in streamwise and vertical mean velocity is shifted earlier in the

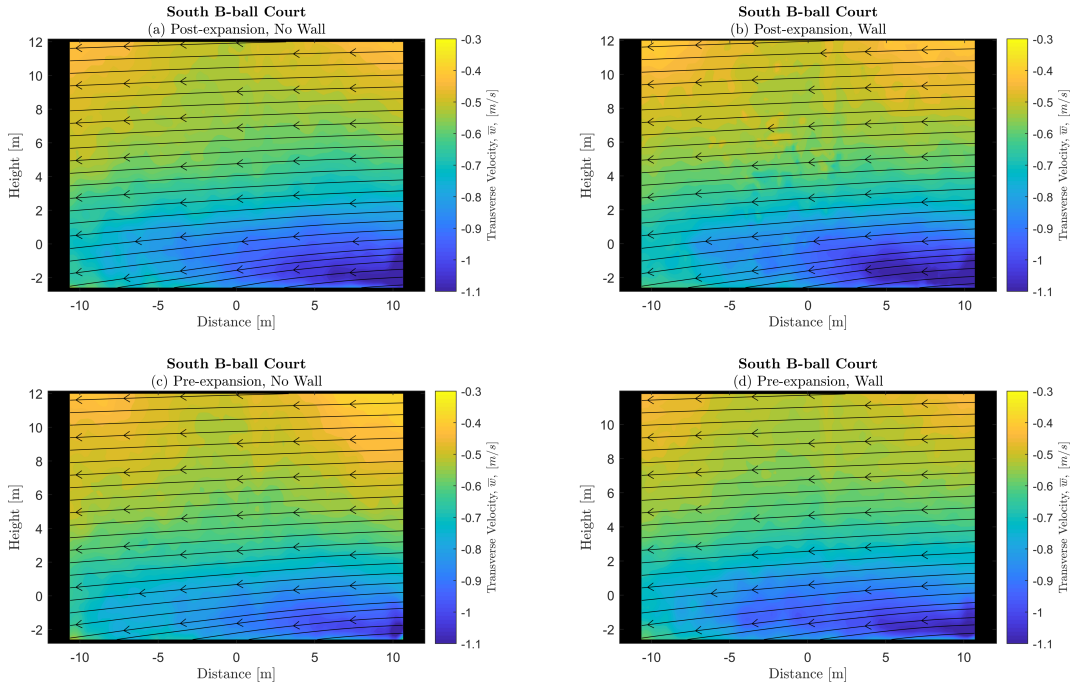

Figure 7: Streamlines of mean in plane velocity components, $\bar{u}$, and $\bar{v}$ overlaid on the mean out of plane velocity, $\bar{w}$ for the south basket ball court view.

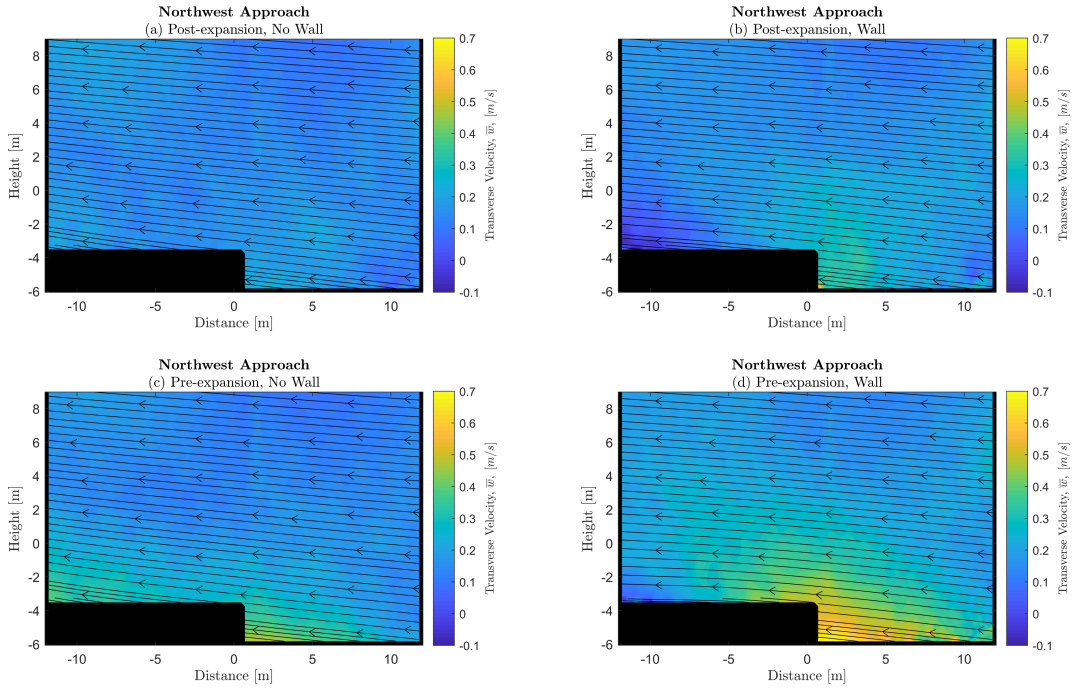

Figure 8: Streamlines of mean in plane velocity components, $\bar{u}$, and $\bar{v}$ overlaid on the mean out of plane velocity, $\bar{w}$ for the northwest approach view.

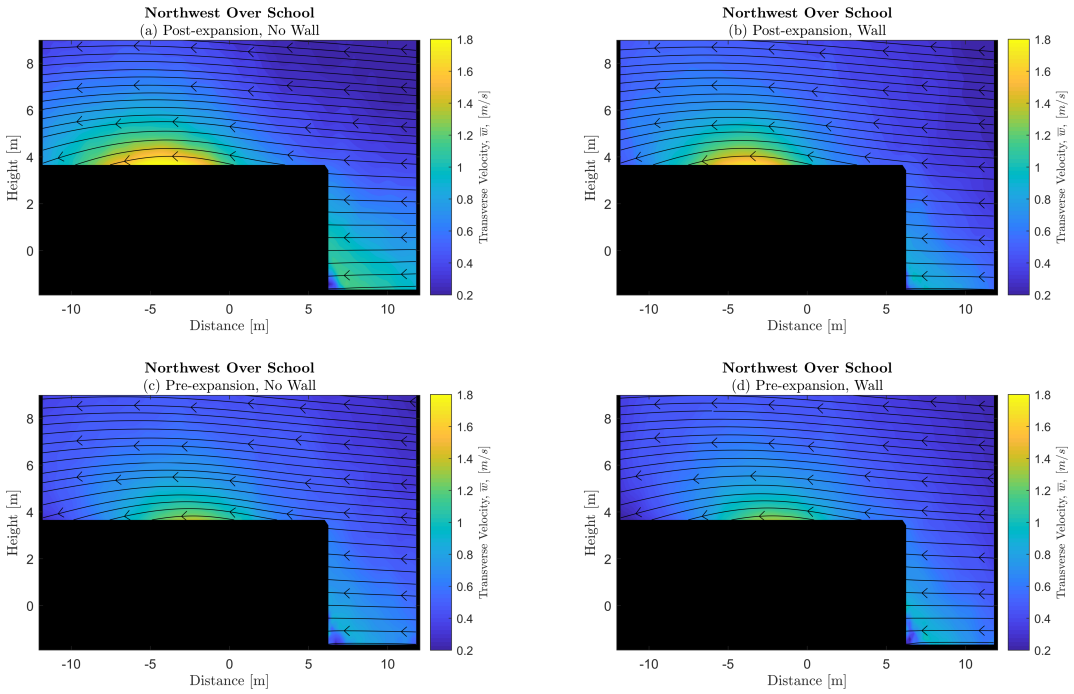

Figure 9: Streamlines of mean in plane velocity components, $\bar{u}$, and $\bar{v}$ overlaid on the mean out of plane velocity, $\bar{w}$ for the northwest over school view.

measurement domain when the wall is included and effects of post-expansion are also visible.

Southwest wind velocities over the school are shown in figure 11 where we see minor changes between flow behaviors for different expansion configurations. The primary differences here are related to the treatment of wall presence, resulting in an increase of out of plane velocities for the configurations with wall present. This effect

Differences between the west approaching wind cases can be seen in figure 12. Although streamlines are generally in the same direction, the angle and complexity is evident. Here, the addition of the wall causes strong recirculation areas and highly complex flow between the school and the wall when present. Flow with increased magnitudes is observed and a near null flow in the moving flow is observed near the ground surface in the presences of the wall. Post-expansion present stronger magnitudes in the streamwise velocity. The maximum vertical velocities are shifted from the top of the room in HTMS to the top of the wall. Stronger magnitudes are observed due to the presence of the wall in the streamwise direction towards HTMS. Note, the western wind was not observed to be the most prominent direction from the Lafayette weather station as shown in figures 1(a) and 1(b). However, this case helps to illustrate possible dynamics and behavior for the instances in which HTMS my be subject to direct imposition by wind flow from the areas west of the freeway.

The over school plane for the western winds is represented in figure 13 and shows similar dependence on wall presence versus the state of expansion in terms of the in plane velocity component, with increased out of plane magnitudes for both expansion cases after wall inclusion. The streamwise and vertical velocities are alleviated over the school with the inclusion of the wall. The post-expansion induces strong magnitude winds in the direction of the school.

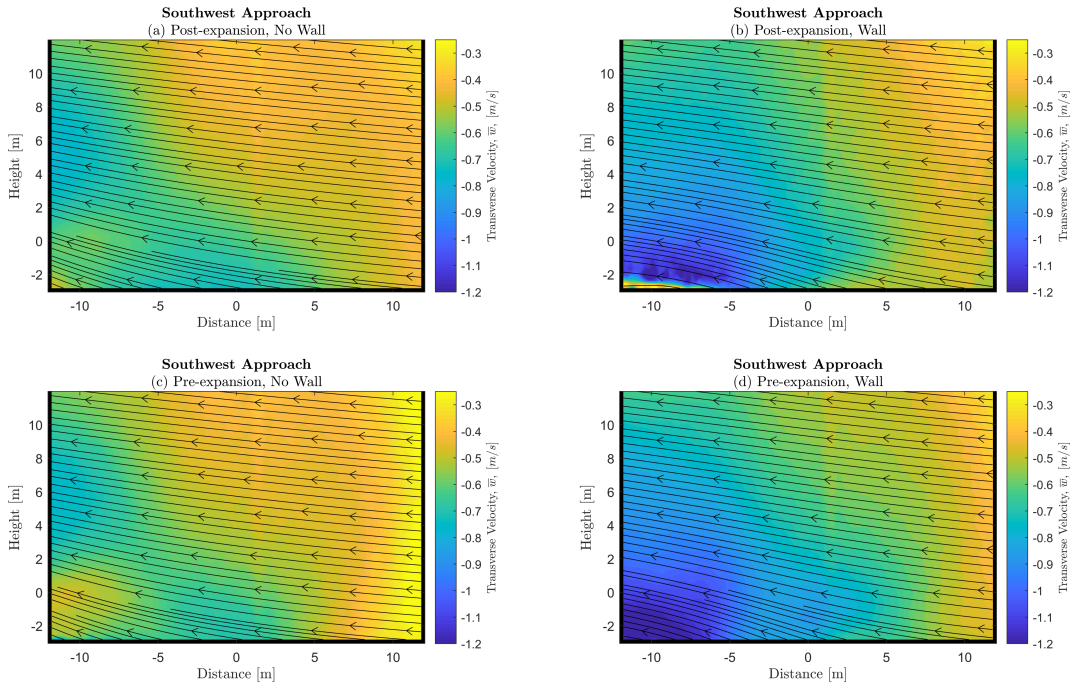

Figure 10: Streamlines of mean in plane velocity components, $\bar{u}$, and $\bar{v}$ overlaid on the mean out of plane velocity, $\bar{w}$ for the southwest approach view.

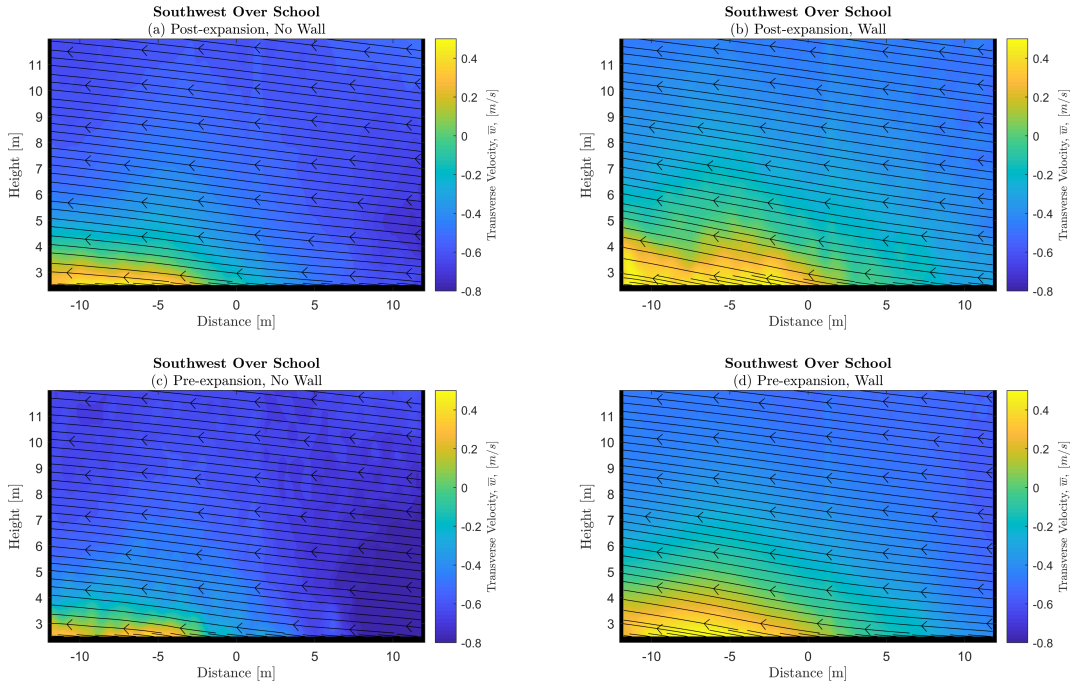

Figure 11: Streamlines of mean in plane velocity components, $\bar{u}$, and $\bar{v}$ overlaid on the mean out of plane velocity, $\bar{w}$ for the southwest over school view.

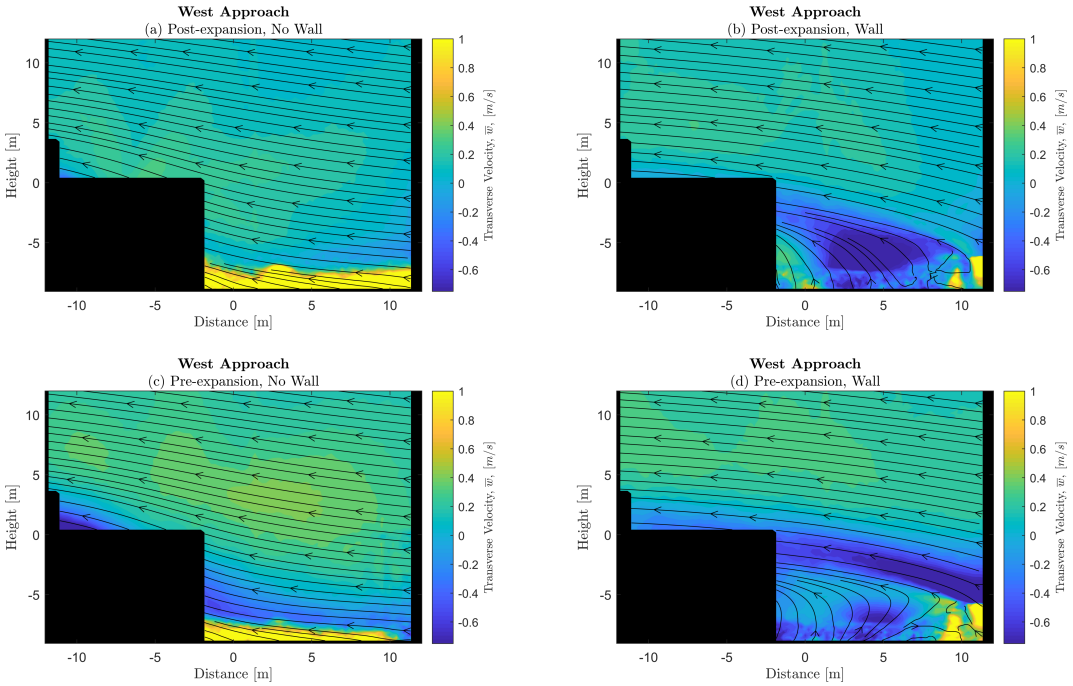

Figure 12: Streamlines of mean in plane velocity components, $\bar{u}$, and $\bar{v}$ overlaid on the mean out of plane velocity, $\bar{w}$ for the west approach view.

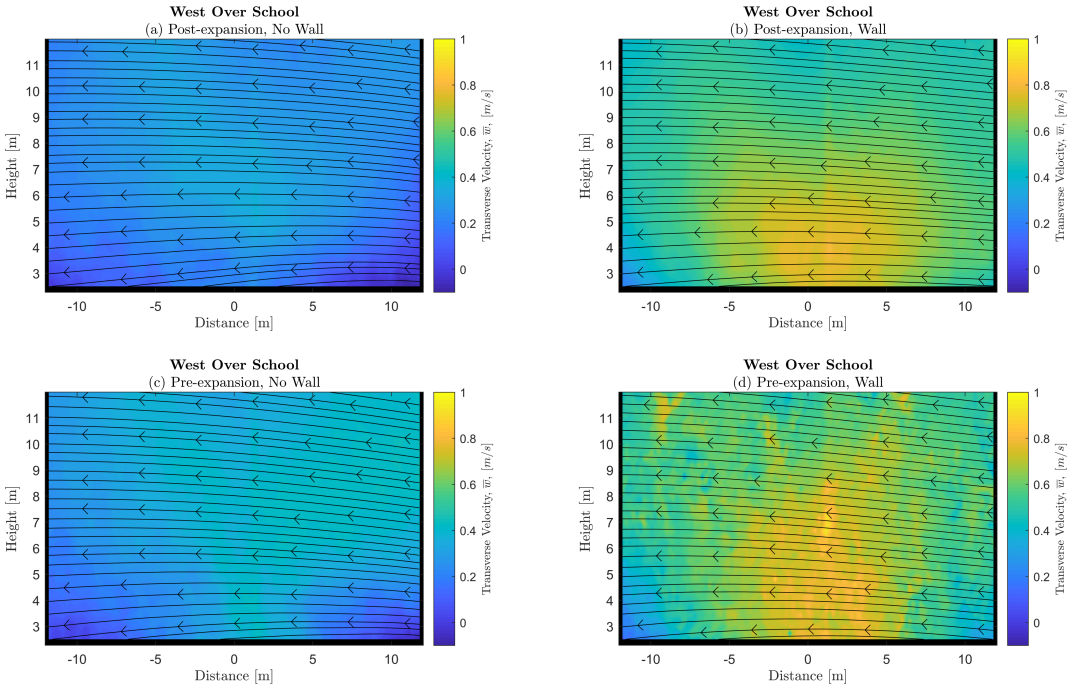

Figure 13: Streamlines of mean in plane velocity components, $\bar{u}$, and $\bar{v}$ overlaid on the mean out of plane velocity, $\bar{w}$ for the west over school view.

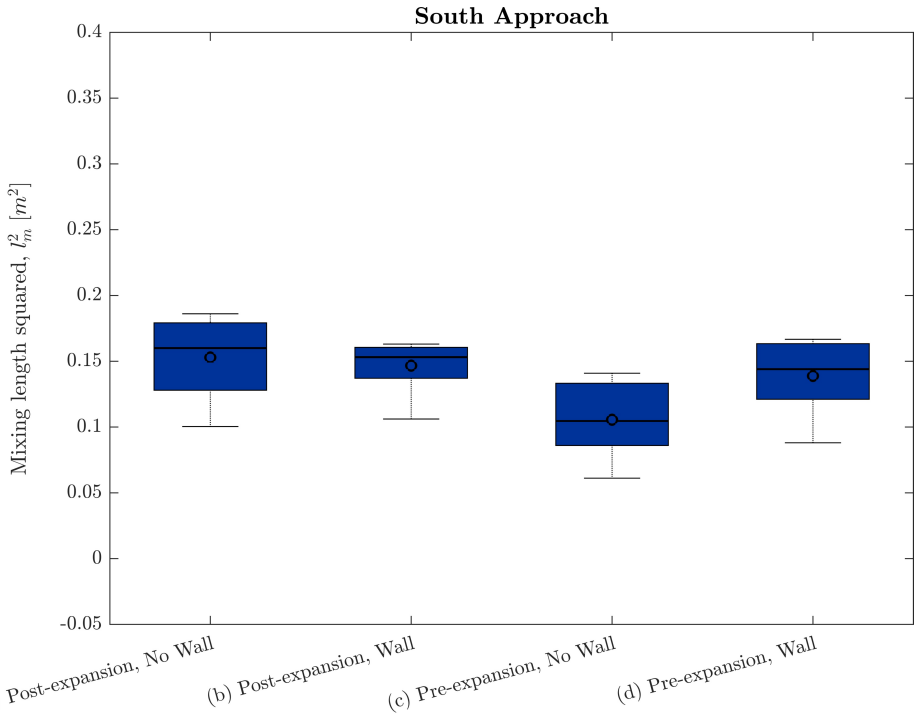

Figure 14: Box plots of mixing length averaged across entire interrogation window of south basketball case.

1.3.2 Mixing length

Turbulence is characterized by the presence of many scales of motion, when considering transport due to large scale motion the mixing length is an appropriate scale to focus on. It is the scale typically used to as a characteristic length scale of momentum transport by fluctuating velocities in the vertical direction of a flow (Tennekes and Lumley (1972)). In flows dominated by a single component of velocity, it is defined as the ratio of Reynolds shear stress to the gradient of the streamwise velocity along the wall-normal direction and given by,

$$l_m^2 = \frac{-\overline{u'v'}}{\left|\frac{\partial \bar{u}}{\partial y}\right| \frac{\partial \bar{u}}{\partial y}}. \tag{1}$$

Figures 14 through 19 show the square of the mixing length averaged in the streamwise direction across the interrogation windows for all cases except the southwest direction. The southwest direction is omitted because the mixing lengths are negligible compared to the other cases. The box plots show the distribution of the mixing length across the height of the interrogation window and how the distribution changes across the four different treatments considered. This analysis allows for inferences to be made as to how the treatments affect the mixing length. The box plots representing the distributions show five quantities for every treatment, the solid line within the box represents the median, the dot, the mean, the upper and lower edges of the box represent the second and third quartiles respectively, and the fences outside the box are both 1.5 inner-quartile ranges away from the box boundaries.

In the south approach case, shown in figure 14 small variations are present in the mixing length distributions across the treatments. All four distributions are generally tight and the medians generally fall near or on the means. A slight increase in the mean values is seen in the post-expansion cases, though the effect is

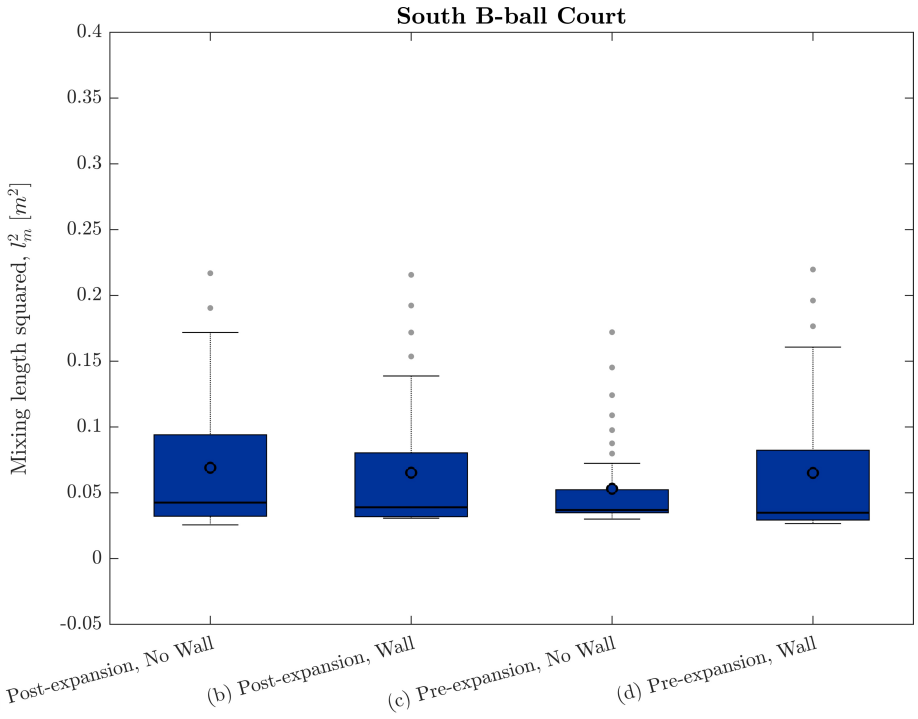

Figure 15: Box plots of mixing length averaged across entire interrogation window of south approach case.

slight. It should also be noted that the mean is increased slightly on the pre-expansion cases in the presence of the wall, though the mean and median still fall below those of the post-expansion cases. In these data, the presence of a wall has less effect than the expansion, though the increase is marginal in the expansion cases.

The mixing length distributions in the south basketball court view, figure 15 all present large positive extreme values, these are likely due to boundary layer perturbations from the roofline of the school upstream of where these data were captured, this is reasonable as they appear across all the cases, so are likely not a result of the treatments. Quite similar mean and median values are seen across all treatments. The pre-expansion no wall case shows a very tight distribution of data, with the lowest mean. In contrast, the addition of the wall in the pre-expansion case dramatically expands the distribution.

Contrary to what was seen in the south cases, the post-expansion cases show the tightest distributions with the lowest means and medians in the west approach data found in figure 16. The pre-expansion no wall treatment shows a distribution similar to that seen in the west over school and northwest approach cases shown in figures 17 and 18 respectively. This case is striking in that a dramatic increase in the spread of data and the mean is seen in the pre-expansion case in the presence of the wall while the median is still low, indicating a skewed distribution with large values of relatively low frequency.

As is the case with the west approach distributions, the post-expansion treatments in the west over school data in figure 17 show tighter distributions and lower means and medians than the pre-expansion treatments. While the post-expansion no wall treatment shows the highest values, these outliers do not speak to a general trend towards larger values. The pre-expansion no wall treatment shows the highest values. The very large increase in the pre-expansion wall case seen in the west approach view is not seen here, this plane is significantly farther away from, and higher up than the approach case, so the immediate effects of the presence of the wall diminish when the flow progresses over the school.

The distributions in the northwest approach direction of figure 18 show small variation across treatments.

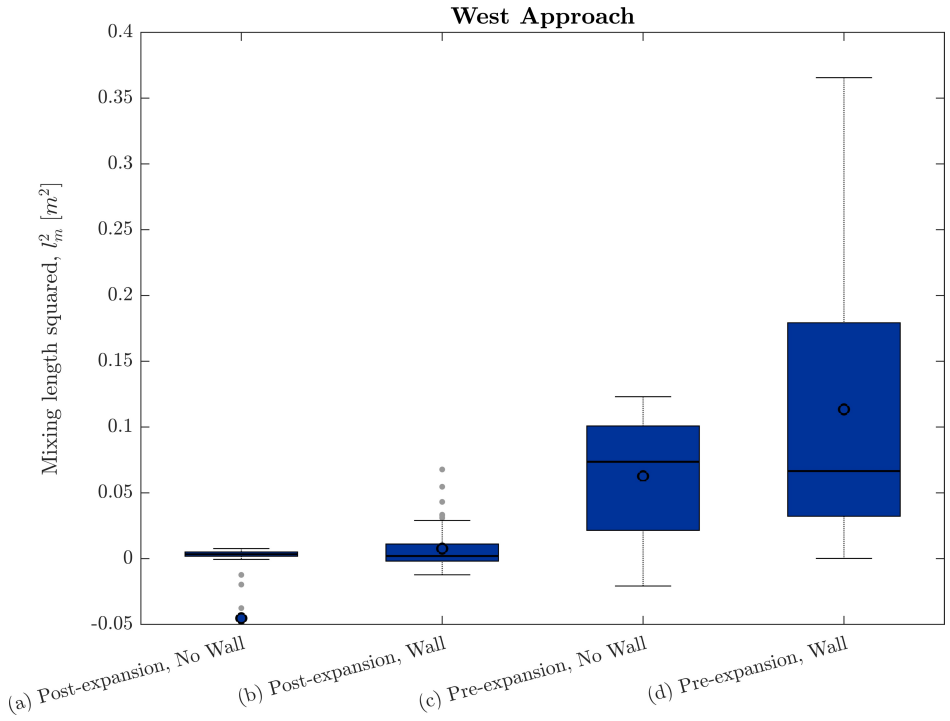

Figure 16: Box plots of mixing length averaged across entire interrogation window of west approach case.

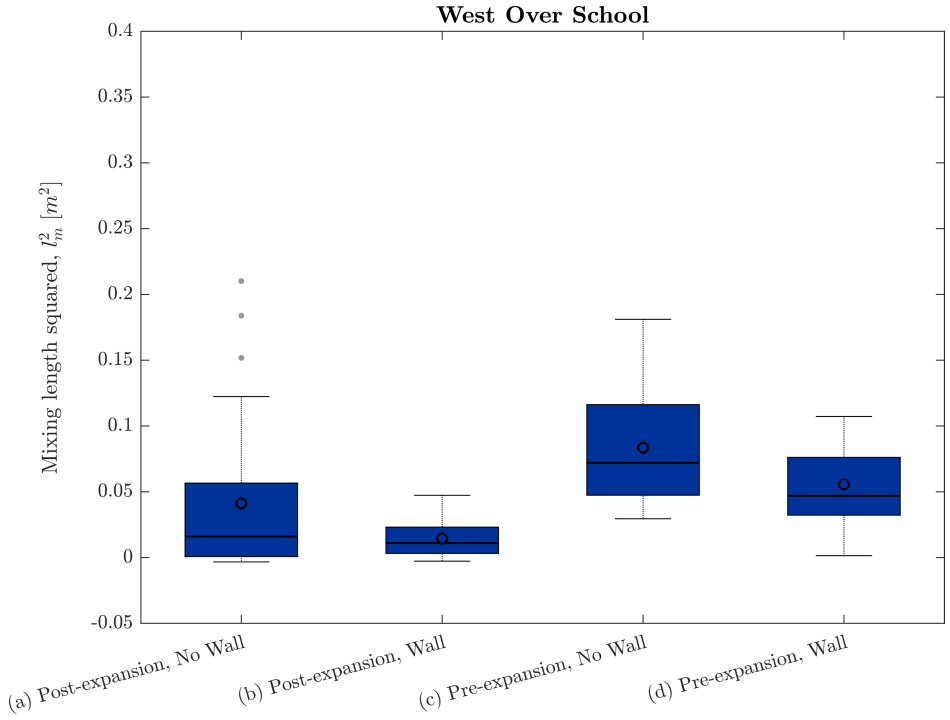

Figure 17: Box plots of mixing length averaged across entire interrogation window of west over school case.

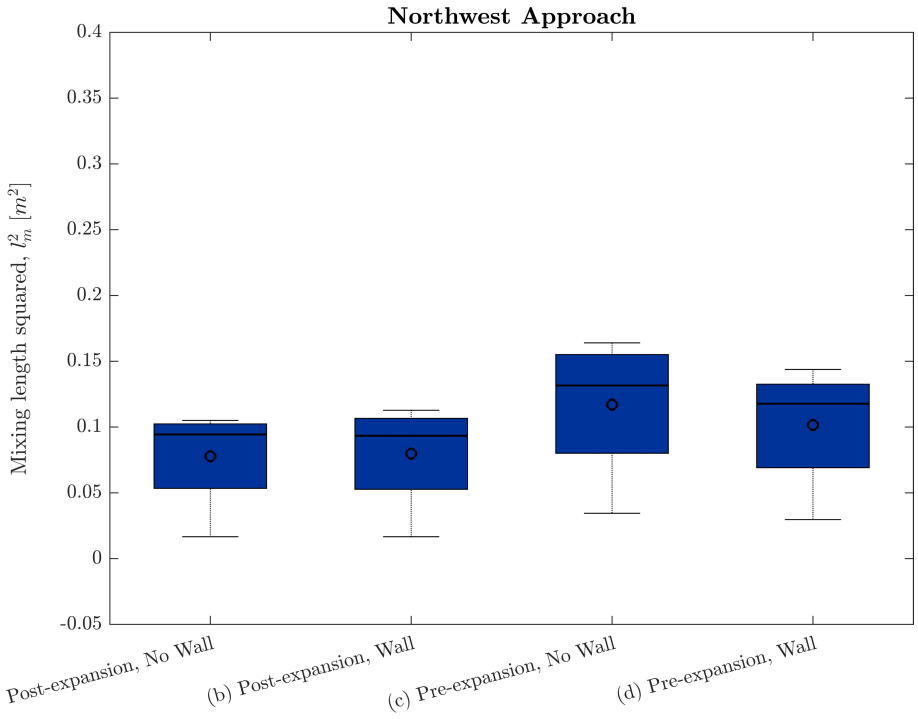

Figure 18: Box plots of mixing length averaged across entire interrogation window of northwest approach case.

Again the post-expansion cases have slightly lower means and medians compared to the pre-expansion treatments. The pre-expansion no wall case shows the widest distribution and highest values.

The northwest over school view in figure 19 shows a different trend across treatments than was seen in the west and northwest approach cases. Similar to the two south directions, the means and medians are slightly higher in the pose-expansion treatments. Further a slight negative effect is seen in the pre-expansion wall treatment.

The infiltration rates reported are based on US Department of Energy recommendations and are calculated based on a wind velocity correction to a known leakage rate at 75 pa, $I_{p75} = 1.8\, cfm/ft^2$ Gowri et al. (2009). Infiltration is calculated as

$$I_{pavg} = I_{p75}\left(\frac{P_{avg}}{75}\right). \tag{2}$$

P_{avg} is the average pressure at the eve height of a building, $P_{avg} = 0.5\, C_s\, \rho\, U_H^2$, where U_H is the wind speed at eve height, and $C_s = 0.1617$, an empirical coefficient. The box plots shown in figures 20 through 22 show the distributions of infiltration rates based on a 5x5 matrix of streamwise velocity values centered at the eve height of the school, the matrix spatially averaged to a point, the distributions represent the temporal variation in this spatial average across the 700 PIV snapshots. In the following discussion when percent differences are cited they are calculated between two treatments as $(T_1 - T_2)/\frac{T_1+T_2}{2} \times 100$ and are therefore relative percent differences between the two cases discussed.

The infiltration rates across treatments in the case of southerly winds found in figure 20 show mixed results in the presence of the wall between the pre and post expansion treatments. In the pre expansion cases the wall reduces the mean infiltration rate by 13%, while in the post-expansion, the mean value is increased by 3%. The minimum mean value across all treatments is in the post-expansion no wall case, which is 16% lower than the pre-expansion no wall case, suggesting that in the southerly winds, the freeway expansion

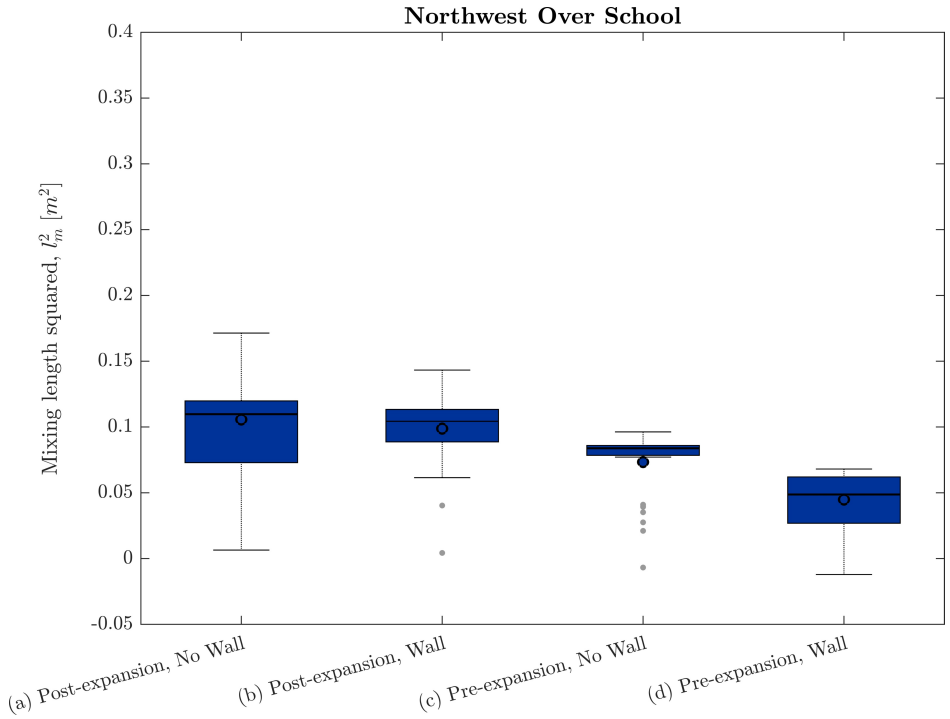

Figure 19: Box plots of mixing length averaged across entire interrogation window of northwest over school case.

will have a positive impact on the infiltration rate.

In the case of winds from the west, a good correlation between the data in infiltration rates is found in figure 21 and the mixing lengths seen in figure 16. In both figures, the presence of a wall either reduces the infiltration rate, or increases the mixing length compared to the cases without the wall. The infiltration rate data show 25% reductions between the no wall and wall cases in both the pre and post expansion treatments. The lowest infiltration rate seen in the west approach data is in the pre-expansion wall case, which is 25% less than the post-expansion wall case. In the case of winds coming from the west, while the infiltration rate is generally lower in the pre-expansion treatment, in both free-way setups the presence of a wall dramatically decreases the infiltration rate.

The infiltration rates seen in the case of winds from the northwest, figure 22, slightly increased rates are seen in the wall cases compared to the no wall cases. In the pre-expansion and post-expansion cases we see a 6% and 8% increase in the means, respectively. The minimum mean value falls on pre-expansion no wall, which is 10% less than the maximum value in the post-expansion wall case. It should be noted that while we do see increases in the wall cases, they are relatively small compared to the decreases seen particularly in the westerly winds case.

Figure 23 allows for the means of all the cases to be compared together, the normalization is by the maximum of each case so the values are relative to the specific case. The omitted case, the southwest approach shows negligible change across the treatments. In the northwest approach case, the generally small increases in infiltration rate with the wall cases. The south approach case, which, as seen in figure 1(a), during the autumn and summer represents the most frequent wind direction of the cases considered, shows a decrease in infiltration in the pre-expansion case with the wall. The west approach case, which represents wind events flowing directly across the freeway shows the most dramatic decreases in the presence of the wall, though it should be noted that the wind roses in figures 1(a) and 1(b) show that westerly winds are the least frequent

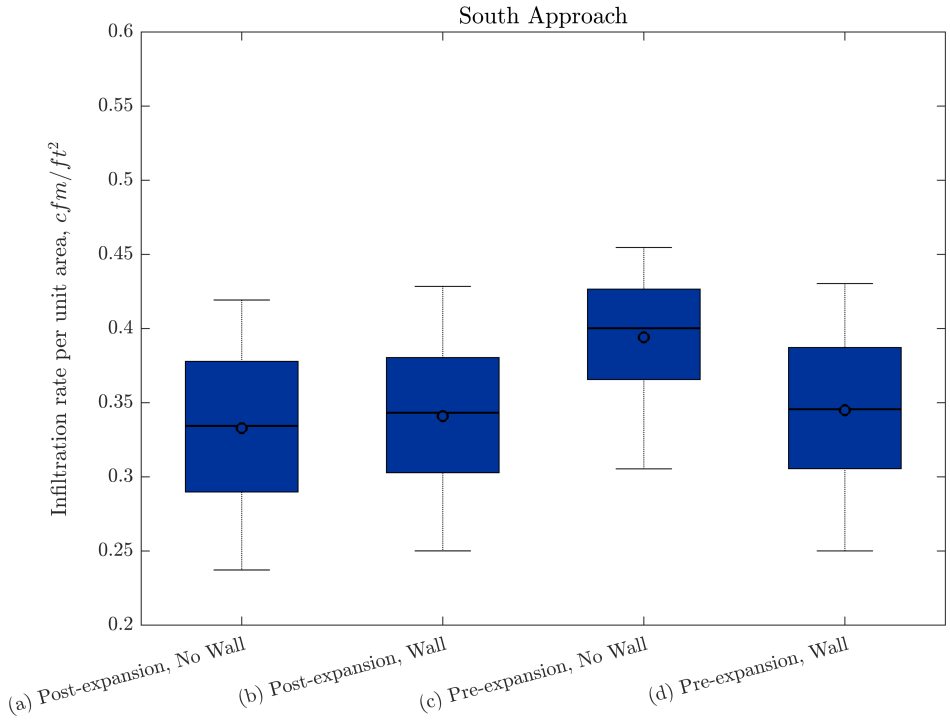

Figure 20: Box plot of infiltration rate per unit area for the south approach case.

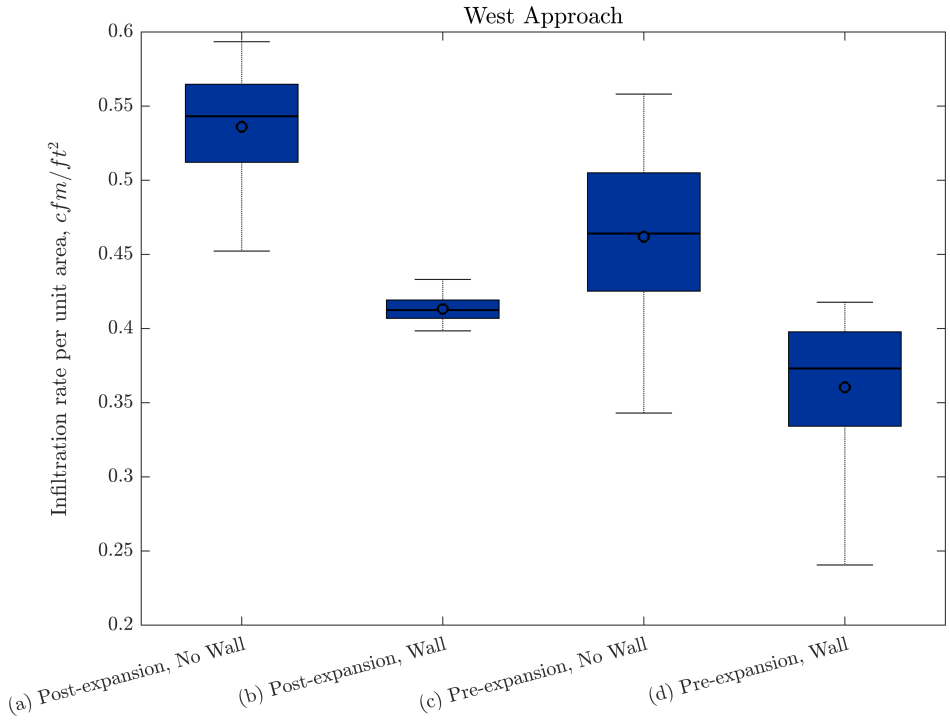

Figure 21: Box plot of infiltration rate per unit area for the west approach case.

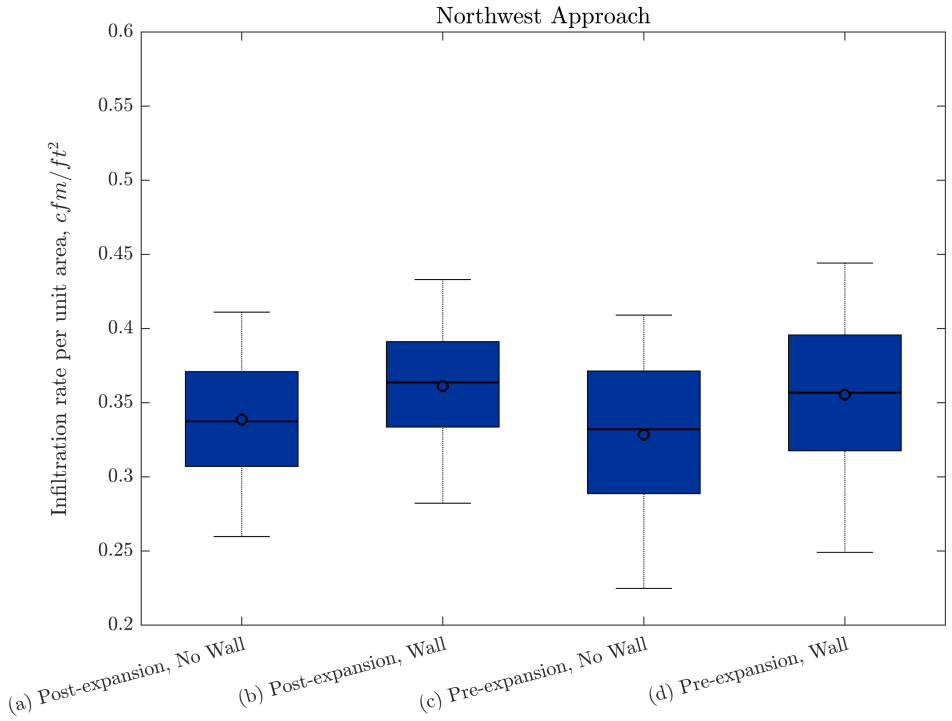

Figure 22: Box plot of infiltration rate per unit area for the northwest approach case.

wind events.

1.4 Outlook

Data are presented for multiple cases where pre- and post- highway expansions are considered as well as the effects due to a wall along the highway in wind tunnel experiments. Mean winds are presented as well as possible indicators, mixing length and infiltration, in order to quantify the differences for a multitude of directions. West direction trends seem to point towards lower infiltration rates and reduced mixing length for the effects of the wall as well as pre-expansion; it should be noted that the wind roses in figures 1(a) and 1(b) show that westerly winds are the least frequent wind events. These variations are not as evident when considering other directions. As mentioned previously, these experiments provide observations in semi-idealized conditions for which effects like atmospheric variations, change in wind magnitudes/direction, further terrain features are not taken into account, but might play a role. Further research in more idealized conditions (two-dimensional geometries) could provide further insight of wall and highway expansion effects. Numerical simulations could serve as a basis of comparison with results obtained in the wind tunnel. The evaluation of vortical motions as well as a three dimensional consideration of the mixing length could also lead to further observations. Full scale testing may be conducted through surrogate/low-cost material for comparison.

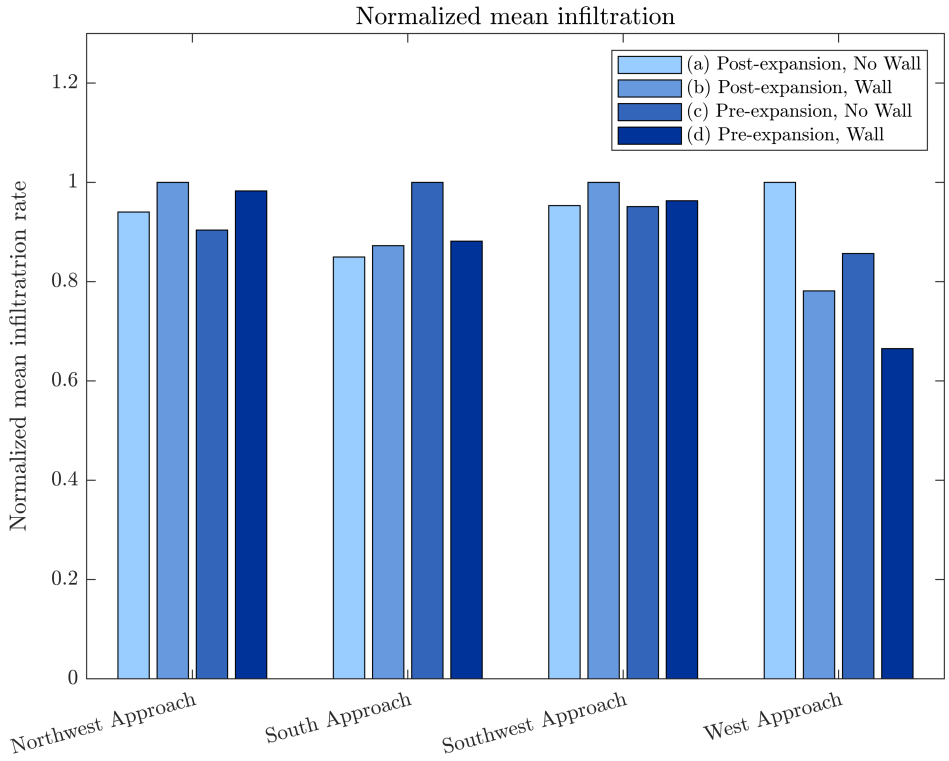

Figure 23: Bar plot of mean infiltration rates normalized by the maximum mean infiltration rate for each view.

References

Abhijith, K. and Gokhale, S. (2015). Passive control potentials of trees and on-street parked cars in reduction of air pollution exposure in urban street canyons. *Environmental Pollution*, 204:99 – 108.

Abhijith, K., Kumar, P., Gallagher, J., McNabola, A., Baldauf, R., Pilla, F., Broderick, B., Sabatino, S. D., and Pulvirenti, B. (2017). Air pollution abatement performances of green infrastructure in open road and built-up street canyon environments – a review. *Atmospheric Environment*, 162:71 – 86.

Akbari, H. (2002). Shade trees reduce building energy use and co2 emissions from power plants. *Environmental Pollution*, 116:S119 – S126.

Baldauf, R. (2017). Roadside vegetation design characteristics that can improve local, near-road air quality. *Transportation Research Part D: Transport and Environment*, 52:354 – 361.

Gallagher, J., Baldauf, R., Fuller, C. H., Kumar, P., Gill, L. W., and McNabola, A. (2015). Passive methods for improving air quality in the built environment: A review of porous and solid barriers. *Atmospheric Environment*, 120:61 – 70.

Gowri, K., Winiarski, D. W., and Jarnagin, R. E. (2009). Infiltration modeling guidelines for commercial building energy analysis. Technical Report PNNL-18898, 968203.

Hagler, G. S., Lin, M.-Y., Khlystov, A., Baldauf, R. W., Isakov, V., Faircloth, J., and Jackson, L. E. (2012). Field investigation of roadside vegetative and structural barrier impact on near-road ultrafine particle concentrations under a variety of wind conditions. *Science of The Total Environment*, 419:7 – 15.

Janhäll, S. (2015). Review on urban vegetation and particle air pollution – deposition and dispersion. *Atmospheric Environment*, 105:130 – 137.

Pugh, T. A. M., MacKenzie, A. R., Whyatt, J. D., and Hewitt, C. N. (2012). Effectiveness of green infrastructure for improvement of air quality in urban street canyons. *Environmental Science & Technology*, 46(14):7692–7699. PMID: 22663154.

Tennekes, H. and Lumley, J. L. (1972). *A First Course in Turbulence*. MIT Press.

Vos, P. E., Maiheu, B., Vankerkom, J., and Janssen, S. (2013). Improving local air quality in cities: To tree or not to tree? *Environmental Pollution*, 183:113 – 122. Selected Papers from Urban Environmental Pollution 2012.

Wania, A., Bruse, M., Blond, N., and Weber, C. (2012). Analysing the influence of different street vegetation on traffic-induced particle dispersion using microscale simulations. *Journal of Environmental Management*, 94(1):91 – 101.

Yang, J., McBride, J., Zhou, J., and Sun, Z. (2005). The urban forest in beijing and its role in air pollution reduction. *Urban Forestry Urban Greening*, 3(2):65 – 78.

Yang, J., Yu, Q., and Gong, P. (2008). Quantifying air pollution removal by green roofs in chicago. *Atmospheric Environment*, 42(31):7266 – 7273.